Dynamic Scaling of Colloidal Gel Formation at Intermediate Concentrations

Qingteng Zhang (□□□), Divya Bahadur, Eric M. Dufresne, Pawel Grybos, Piotr Kmon, Robert L. Leheny, Piotr Maj, Suresh Narayanan, Robert Szczygiel, Subramanian Ramakrishnan, and Alec Sandy

Phys. Rev. Lett. **119**, 178006 — Published 25 October 2017

DOI: 10.1103/PhysRevLett.119.178006

Dynamic Scaling of Colloidal Gel Formation at Intermediate Concentrations

Qingteng Zhang,[1] Divya Bahadur,[2] Eric M. Dufresne,[1] Pawel Grybos,[3] Piotr Kmon,[3] Robert L. Leheny,[4] Piotr Maj,[3] Suresh Narayanan,[1] Robert Szczygiel,[3] Subramanian Ramakrishnan,[2,*] and Alec Sandy[1,†]

[1] *X-Ray Science Division, Argonne National Laboratory, Lemont, IL 60439, USA*
[2] *Chemical and Biomedical Engineering, FAMU-FSU College of Engineering, Tallahassee, FL 32310, USA*
[3] *AGH University of Science and Technology, av. Mickiewicza 30, Krakow 30-059, Poland*
[4] *Department of Physics and Astronomy, Johns Hopkins University, Baltimore, MD 21218, USA*

(Dated: September 22, 2017)

We have examined the formation and dissolution of gels composed of intermediate volume-fraction nanoparticles with temperature-dependent short-range attractions using small-angle x-ray scattering (SAXS), x-ray photon correlation spectroscopy (XPCS), and rheology to obtain nanoscale and macroscale sensitivity to structure and dynamics. Gel formation after temperature quenches to the vicinity of the rheologically-determined gel temperature, $T_{\rm gel}$, was characterized via the slow-down of dynamics and changes in microstructure observed in the intensity autocorrelation functions and structure factor, respectively, as a function of quench depth ($\Delta T = T_{\rm quench} - T_{\rm gel}$), wave vector, and formation time t_f. We find the wave-vector-dependent dynamics, microstructure, and rheology at a particular ΔT and t_f map to those at other ΔTs and t_fs via an effective scaling temperature, T_s. A single T_s applies to a broad range of ΔT and t_f but does depend on the particle size. The rate of formation implied by the scaling is a far stronger function of ΔT than expected from the attraction strength between colloids. We interpret this strong temperature dependence in terms of cooperative bonding required to form stable gels via energetically favored, local structures.

During gelation, the gel-forming constituents form a system spanning network and the storage modulus of the material changes by several orders of magnitude upon only a slight change in the strength of interparticle attractions [1]. Gels formed of colloidal nanoparticles are widely studied examples of such intriguing materials because fundamental aspects of their behavior can be systematically explored through variation of particle size, coating and the surrounding medium among many other variables [2]. At high volume fractions ($\phi \gtrsim 0.5$), such suspensions also provide insight into processes such as crystallization and the glass transition [3] while at lower volume fractions ($\phi \lesssim 0.1$) they yield knowledge about materials with self-similar or fractal structures [4]. Suspensions in the intermediate volume fraction regime ($0.1 \lesssim \phi \lesssim 0.5$) are relevant to understanding the role of spinodal decomposition and arrested phase separation in gel formation and are an area of active investigation [3, 5–13]. For example, the percolated particle network in the final gel state at intermediate concentrations has been measured, directly or indirectly, via experimental methods such as confocal microscopy [14–17], ultra-small-angle x-ray-scattering [18] and rheology [11, 19–21] and also simulated using molecular dynamics (MD) [22–25]. Far less studied are the formation and dissolution processes in gels; thermo-reversible colloidal gels are ideal for such investigations because particle interactions can be finely and abruptly tuned via sudden temperature changes.

Understanding gels is challenging because of their sensitivity to small changes in control parameters, heterogeneity in their structure and dynamics, and because their properties change with time as a gel forms and ages. Advancing experimental knowledge of these materials requires a probe with spatial sensitivity to the scale of the nanoparticle size ($\sim$ 100 nm) and temporal sensitivity to the scale of the diffusion time ($\sim$ 10 μs). The recent development of an ultra-fast, x-ray-photon-counting, pixel-array detector (UFXC32k) [26, 27], has enabled high-fidelity recording of x-ray speckle patterns with time resolution of 20 μs. This detector permits the observation of nanoscale fluctuations in colloidal systems across a broad dynamic range that was previously inaccessible. Combining this tool with separate macroscale-sensitive rheology measurements permits a thorough examination of the formation and dissolution of colloidal nanoparticle gels.

In this manuscript, we report x-ray photon correlation spectroscopy (XPCS) studies of intermediate volume fraction, thermo-reversible colloidal gels employing the UFXC32k and companion rheology measurements obtained under the same experimental conditions. The measurements we report were performed either i) as a function of formation time, t_f, after quenches from higher temperatures to the vicinity, ΔT, of $T_{\rm gel}$, where $\Delta T = T_{\rm quench} - T_{\rm gel}$ and $T_{\rm gel}$ is the rheologically-determined gel temperature; or ii) as a function of temperature upon gentle heating after a prolonged dwell following a deep quench. Remarkably, for temperature quenches, we find a simple exponential scaling relationship that connects the structural, dynamic, and rheological behavior at a particular combination of t_f and ΔT with other combinations of the same. We attribute the strong temperature dependence of this scaling to collective behavior associated with the stability of locally favored structures [3] that interconnect to form the percolating gel network.

* sramakrishnan@fsu.edu
† asandy@anl.gov

The thermo-reversible colloidal gels were composed of octadecyl-grafted silica particles with radius $R = 41$ nm and polydispersity of 15% dispersed in decalin at a volume fraction of 0.2. Below the theta temperature of the octadecyl chains in decalin, $T_\theta = 306$ K, the particles exhibit a temperature-dependent short-range attractive interaction [18]:

$$U(T) = Ak_{\mathrm{B}}(T - T_\theta) \tag{1}$$

where $A \approx 30$, leading to gel formation at sufficiently low temperature. The gel point, $T_{\mathrm{gel}} = 278.4$ K, is determined from rheology as the temperature at which the loss modulus G'' is equal to the storage modulus G' when the gel is slowly heated from well within the gel state [19]. Gelation was induced via thermal quenches starting from room temperature, where the suspensions approximate hard-sphere fluids, and ending at a temperature in the vicinity of T_{gel}. The cooling rate was 3 K/min, and the temperature undershoot was less than 0.05 K. The temperature was then held constant during which time the gel slowly forms. Fluctuating speckle patterns from the scattered coherent x-ray beam were recorded with the UFXC32k detector. Total acquisition times were limited to 6 seconds or less ($\leq 3 \times 10^5$ frames) based on the memory in the detector control unit. Such measurements were repeated approximately every 30 seconds with the beam at a new location on the sample to reduce possible radiation-induced effects. Since the formation times were long compared to the acquisition time, each measurement was effectively a "video clip" of the dynamic behavior at a particular t_f. As shown below, the measurements captured well the dynamical evolution of gel formation; however, the slow aging behavior observed previously in well-formed colloidal gels [4, 19, 28–35] was outside the scope of the measurements and, hence, not a part of this study. Technical details regarding the sample preparation and the rheology and XPCS measurements can be found in the Supplemental Materials [36].

Figure 1(a) shows time-averaged small-angle x-ray scattering (SAXS) images acquired shortly (bottom, $t_f =$ 30 s) and well after (top, $t_f = 10^4$ s) a quench to $\Delta T = -1$ K. The speckle structure is washed away at small t_f because of the fast Brownian motion of the nanoparticles that are still fluid, while finely-structured speckles are apparent at large t_f because of arrested nanoparticle motion in the gelled state. Fig. 1(b) shows the structure factor $S(QR)$, where Q is the scattering wave vector, calculated from the images in Fig. 1(a). $S(QR)$ is obtained by azimuthally averaging the scattering intensities shown in Fig. 1(a) around the origin of reciprocal space, dividing these by the same averages obtained from a dilute sample and then normalizing so that $S(QR)$ goes to 1 in the large Q limit [37]. Comparing the transition of $S(QR)$ profiles obtained from the more fluid (black plus signs) states to more gelled (black crosses) states, we find that $S(QR)$ increases in magnitude at small Q and the peak in $S(QR)$ shifts to higher Q [22, 23, 38] indicative of the colloids forming the elementary building blocks of the gel at early stages of gelation (see Fig. S2).

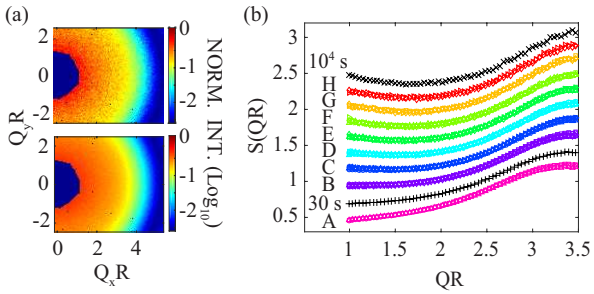

FIG. 1. (Color online) (a) Average scattering patterns acquired after formation times of 30 s (bottom) and 10^4 s (top) following a quench to $\Delta T = -1$ K. The blue polygons near $Q = 0$ are shadows of the beamstop and are not included in the data analysis. (b) The structure factor at various formation times. The black plus signs and crosses correspond to the data in (a) at formation times of 30 s and 10^4 s, respectively. The rainbow-colored data sets (labelled A–H) are explained in the text. Each set of data except the bottom (set A) is vertically shifted by 0.2 from its neighbor for clarity.

The dynamical evolution of the gel formation process is revealed directly by the growing characteristic timescale and changing lineshape of the normalized intensity time autocorrelation functions $\Delta g_2(Q,t) = [g_2(Q,t) - 1]/[g_2(Q, t \to 0) - 1]$ calculated from speckle pattern sequences obtained at different t_f. Figure 2 displays a set of 31 correlation functions at $Q = 1.2/R$ and various ΔT and t_f, in which different quench depths are represented by different symbol shapes (from diamonds to circles). For each quench depth, multiple correlation functions at different t_f are shown using different symbol colors. Figure 3 displays the values of t_f and ΔT corresponding to the color-coded symbols in Fig. 2. The correlation functions capture the evolving nanoscale dynamics after each quench, from behavior characteristic of an ergodic fluid at early t_f (set A in Fig. 2) to a partial decay indicating localized dynamics of a well-formed gel [39] at late t_f (set H in Fig. 2).

As Fig. 3 illustrates, the values of t_f over which this dynamical evolution occurs decrease by orders of magnitude as the quench temperature is decreased by ≤ 1.5 K. Remarkably, despite this large range in the rate of gel formation, the collapse of the correlation functions at different ΔT onto the same family of curves in Fig. 2 demonstrates that the system passes through dynamically equivalent intermediate states during gelation. This equivalence of the intermediate states (A–H) is also found in the static structures, as shown in Fig. 1b where all 31 corresponding $S(QR)$ are arranged and plotted in the same way as Fig. 2 and excellent matching of $S(QR)$ is observed at each intermediate state. Also striking is how only small changes in particle interaction strength, listed along the top axis of Fig. 3 as obtained from Eq. (1), produce such dramatic changes in the rate of gel formation.

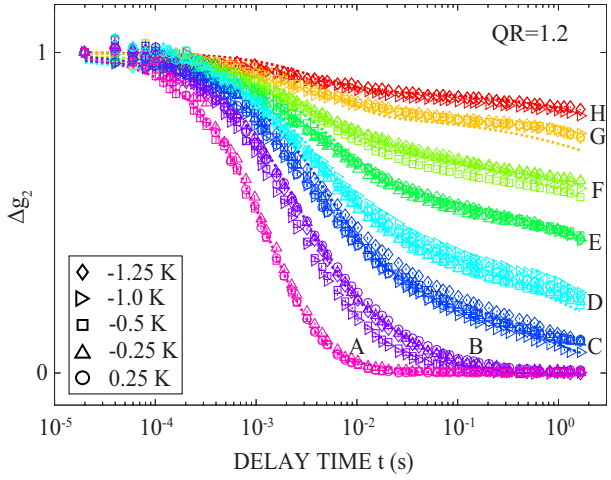

FIG. 2. Correlation functions at $QR = 1.2$ tracking the evolving dynamics following temperature quenches. The error bars are smaller than the markers for most of the data. Each capital letter labels a family of nearly identical correlation functions obtained at different t_f and ΔT (see Fig. 3). The dotted lines are guides-to-the-eye.

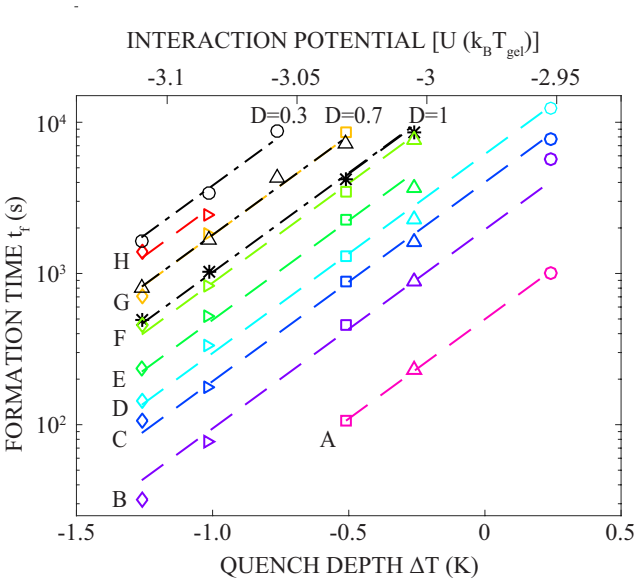

FIG. 3. Families of formation times and quench-depths at which the XPCS correlation decays and structure factors match in Figs. 2 and 1(b), respectively. Each colored symbol indicates the t_f and ΔT of the data set in Figs. 2 and 1(b) with the same shape and hue. The colored dashed lines are fit results using Eq. (2), as discussed in the text. The black stars, triangles and circles and the black dot-dashed lines are from rheology measurements discussed in the text. The interaction potential along the top x-axis is calculated from Eq. (1).

We note that although Fig. 2 shows $\Delta g_2(Q,t)$ at only $QR = 1.2$, the matching of the curves was performed by minimizing the reduced χ^2 among the correlation functions over the full measurement range, $1.2 \leq QR \leq 3$ (see Fig. S1). Thus, the mapping between t_f and ΔT that leads to the collapse of the curves in Fig. 2 is independent of wave vector [40].

The successful overlay of different Δg_2s and $S(QR)$s implies a scaling relationship between ΔT and the time required to reach different points in the gel formation, which the parallel dashed lines in Fig. 3 indicate is exponential. Specifically, the lines are the result of a fit using:

$$t_f^{\alpha}(\Delta T) = t_{f_0}^{\alpha} \cdot \exp\left(\frac{\Delta T}{T_s}\right), \qquad (2)$$

where $T_s = 0.33$ K is a scaling temperature that is common to all families of Δg_2s, the superscript α denotes points in the evolution displaying similar dynamics (i.e., points corresponding to one of the curves A–H in Fig. 2), and $t_{f_0}^{\alpha}$ are reference times related to the time scales of gel formation following a (hypothetical) quench to $\Delta T = 0$. The dashed lines provide an excellent description of the observed formation times versus quench depths over the full range of ΔT probed, -1.25 K $\leq \Delta T \leq$ 0.25 K (see the Supplemental Materials [36] for a discussion of alternative fitting models, including power-law scaling, for the data in Fig. 3).

We also performed rheology measurements, at frequency $\nu = 1$ Hz, after quenches like those described above. During gelation, G' and G'' increase with t_f, and the dissipation factor, $D = G''/G'$, decreases. The gel point can be identified as the time when $D = 1$, which Negi *et al.* [21] have shown occurs at a t_f that is independent of ν. The black stars in Fig. 3 show the gel points in our measurements. Consistent with previous work [21], we find G' and G'' as a function of t_f at different ΔT can be scaled. This scaling is illustrated by the black triangles and circles in Fig. 3, which show the t_f at which D reaches 0.7 and 0.3, respectively, at different ΔT. The black dot-dashed lines in the figure, which pass through the data for each D, are guides-to-the-eye with the same slope as the XPCS-derived data demonstrating that the same exponential scaling relates the rate of gel formation to ΔT in the evolving rheology.

A key question raised by the exponential scaling in Fig. 3 is the dramatic dependence of the formation rate on the strength of the interparticle potential. Previous work has shown that gelation in nanocolloidal suspensions with weak short-range attraction is driven by percolation [10, 21] through reversible bonding that resembles reaction-limited cluster aggregation (RLCA) [41, 42]. However, models for such gelation predict an exponential dependence of rate of formation on interparticle potential that is markedly weaker than the dependence in Fig. 3 [41, 43]. A possible explanation for the observed strong dependence comes from considering the assembly of particle clusters as precursors to gel formation. Examining the structure of intermediate-concentration gels using microscopy and simulations, Royall *et al.* [3] identified a distinct set of low-energy packings comprised of

5 to 13 particles, which they labelled "locally favored structures" (LFS), as the primary building blocks of percolating gel networks. If we take the breaking of particle bonds to be thermally activated, we find the lifetime τ of such a cluster to be $\tau = 1/[f\exp(NU/k_{\rm B}T)]$, where f is an attempt frequency, U is the bond strength per Eq. (1), and N is the average number of bonds in a LFS. Taking $T_{\rm quench}$ as a small excursion ΔT from $T_{\rm gel}$, so that $1/T \approx 1/T_{\rm gel} - \Delta T/T_{\rm gel}^2$, we obtain $\tau \propto \exp\{-\Delta T/[T_{\rm gel}^2/(ANT_\theta)]\}$. Further, assuming that the population of LFSs is proportional to τ and that the gel formation rate is proportional to the LFS population, we arrive at $t_f^\alpha \propto \exp\{\Delta T/[T_{\rm gel}^2/[(ANT_\theta)]\}$. Comparing the denominator of this result to Eq. (2), we make the assignment $T_s = T_{\rm gel}^2/(ANT_\theta)$ and with $T_s = 0.33$ K as determined per Fig. 3, we find $N \approx 26$, which is a reasonable value for the number of bonds in a LFS (For comparison, the smallest, 5-particle LFS identified by Royall *et al.* has 10 bonds, while an icosahedron, which is a commonly invoked preferred local packing of attractive spheres, has 36 bonds). Notably, this interpretation of the scaling in Fig. 3 implies that a single value of N is sufficient to describe the formation rate over a wide dynamic range, indicating that it is the geometric considerations of packing, which are invariant to the quench depth, that are relevant to the gel formation. Indeed, similar behavior was observed in Ref. 3, where the size distribution of LFSs changed little as the particle interaction strengths were varied.

Similar quench measurements were performed on a second suspension with 56-nm-radius colloids, and the correlation decay and scaling plots akin to Figs. 2 and 3 are shown in Fig. S3 in the Supplemental Material [36]. The same scaling behavior is found but with $T_s = 0.45$ K and $N = 19$. The size dependence of N is likely associated with differences in the preferred topologies of LFSs, which can vary with the interaction range normalized by the particle size [44].

We note that the exponential scaling, while valid for both particle sizes over the range of quench depths probed, -1.25 K $\leq \Delta T \leq 0.25$ K, must break down at lower and higher ΔT. For quenches to temperatures above the gel point, dynamic arrest will not occur even for arbitrarily large t_f. (See Supplemental Materials [36] for a discussion of the divergence of t_f.) In this regard, the extension of the scaling in Fig. 3 to $\Delta T > 0$ is interesting since it suggests that the same evolution in particle-scale dynamics that characterizes incipient gel formation could occur following the introduction of weak particle attractions that do not lead to gels. This observation is consistent with the picture associating the slowing dynamics with LFS formation, as Royall *et al.* [3] identify the presence of LFSs in suspensions both above and below the gel transition.

Also, at very low ΔT (deep quench) where the interaction potential is strong compared to k_BT, one should expect that gelation proceeds rapidly with the formation of structures that are less annealed and that rely less on LFSs as building blocks than those formed following shallower quenches. Indeed, MD simulations have shown that instantaneous quenching leads to more disordered gel structures than slower quenches [45]. Consistent with this idea, we found that dynamics were essentially fully arrested, $\Delta g_2(Q,t) \approx 1$ independent of t_f, immediately following a deep quench to $\Delta T = -2.2$ K.

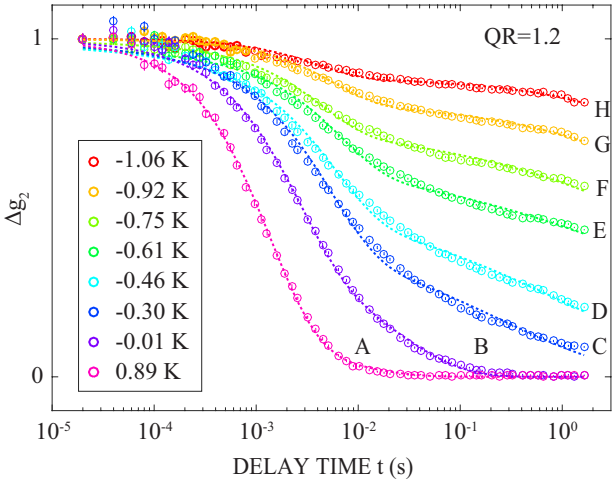

FIG. 4. Normalized correlation decays obtained at $S(QR = 1.2)$. Open symbols are data obtained at the ΔT shown in the legend during slow heating of a gel formed at $\Delta T = -2.2K$. The dotted lines are the same as the ones in Fig. 2.

Differences in the gelation process upon this deep quench compared with the shallower quenches were also reflected in the dynamics observed during gentle heating after forming the gel at $\Delta T = -2.2$ K and holding at that temperature for 30 min. The temperature was increased in steps of 0.15 K with a wait time of 90 s at each step. Figure 4 shows a series of $\Delta g_2(Q,t)$ measured during the heating. The dynamics become progressively faster on heating, even at temperatures well below $\Delta T = 0$, where direct quenches lead eventually to full dynamic arrest. Thus, one can infer that the gel formed following the deep quench becomes structurally unstable when the interparticle attractions are made weaker on heating, and the gel enters a presumably transient period in which it undergoes structural dynamics that would lead to a more stable, better annealed gel. A remarkable feature of the progressively more rapid dynamics induced on heating from the deep quench is the essentially perfect match between the temperature-dependent correlation functions and the correlation functions measured as a function of t_f shown in Fig. 2 following a shallower quench (see Fig. S1 for details on the matching). This match illustrates the universal nature of the dynamic scaling that characterizes the gel formation process.

In conclusion, we have studied the formation and dissolution of thermally-reversible colloidal gels using SAXS, XPCS, and rheology. The dynamic, structural, and rheological signatures of gel formation after quenches display a unified scaling between quench temperature and forma-

tion time. We find that an effective interaction derived from the observed exponential scaling is much stronger than the value obtained by considering only the interparticle potential and is consistent with collective behavior associated with the cooperative bonding needed to initiate and perpetuate gel formation. Such cooperation, with its associated low probability, explains a puzzling aspect of the initiation of gelation, wherein suspensions can remain fluid for very long times (i.e., upwards of 10^4 s at ΔT = -0.25 K in Fig. 3) while possessing microscopic interactions that ultimately drive dynamic arrest into an elastic solid. Simulation studies that access this regime in weakly attractive systems would help deepen our understanding of this key feature of gel formation.

We acknowledge the expert technical assistance of R. Ziegler and helpful conversations with J. Harden, M. Sutton and J. Swan. S.R. thanks the Argonne National Laboratory (ANL) X-ray Science Division Visiting Scientist program for support. S.R. and R.L. acknowledge support from the NSF through CBET-1336166. This material is based upon work supported by Laboratory Directed Research and Development (LDRD) funding from Argonne National Laboratory, provided by the Director, Office of Science, of the U.S. Department of Energy under Contract No. DE-AC02-06CH11357. This research was performed at beamline 8-ID-I of the Advanced Photon Source, a US Department of Energy (DOE) Office of Science User Facility operated for the DOE Office of Science by ANL under contract No. DE-AC02-06CH11357. AGH University of Science and Technology was supported by the National Center for Research and Development, Poland, PBS1/A3/12/2012, in the years 2012–2016.

[1] D. Bonn, H. Kellay, H. Tanaka, G. Wegdam, and J. Meunier, Langmuir **15**, 7534 (1999).
[2] E. Zaccarelli, J. Phys.: Condens. Matter **19**, 323101 (2007).
[3] C. Patrick Royall, S. R. Williams, T. Ohtsuka, and H. Tanaka, Nat. Mater. **7**, 556 (2008).
[4] L. Cipelletti, S. Manley, R. C. Ball, and D. A. Weitz, Phys. Rev. Lett. **84**, 2275 (2000).
[5] S. Manley, H. M. Wyss, K. Miyazaki, J. C. Conrad, V. Trappe, L. J. Kaufman, D. R. Reichman, and D. A. Weitz, Phys. Rev. Lett. **95**, 238302 (2005).
[6] G. Foffi, C. D. Michele, F. Sciortino, and P. Tartaglia, Phys. Rev. Lett. **94**, 078301 (2005).
[7] F. Cardinaux, T. Gibaud, A. Stradner, and P. Schurtenberger, Phys. Rev. Lett. **99**, 118301 (2007).
[8] E. Zaccarelli, P. J. Lu, F. Ciulla, D. A. Weitz, and F. Sciortino, J. Phys.: Condens. Matter **20**, 494242 (2008).
[9] P. J. Lu, E. Zaccarelli, F. Ciulla, A. B. Schofield, F. Sciortino, and D. A. Weitz, Nature **453**, 499 (2008).
[10] A. P. Eberle, N. J. Wagner, and R. Castañeda-Priego, Phys. Rev. Lett. **106**, 105704 (2011).
[11] A. P. R. Eberle, R. Castañeda-Priego, J. M. Kim, and N. J. Wagner, Langmuir **28**, 1866 (2012).
[12] F. Varrato, L. Di Michele, M. Belushkin, N. Dorsaz, S. H. Nathan, E. Eiser, and G. Foffi, Proc. Natl. Acad. Sci. U.S.A. **109**, 19155 (2012).
[13] I. Zhang, C. P. Royall, M. A. Faers, and P. Bartlett, Soft Matter **9**, 2076 (2013).
[14] C. P. Royall, J. Eggers, A. Furukawa, and H. Tanaka, Phys. Rev. Lett. **114**, 258302 (2015).
[15] R. F. Capellmann, N. E. Valadez-Pérez, B. Simon, S. U. Egelhaaf, M. Laurati, and R. Castañeda-Priego, Soft Matter **12**, 9303 (2016).
[16] C. J. Dibble, M. Kogan, and M. J. Solomon, Phys. Rev. E. **74**, 041403 (2006).
[17] C. J. Dibble, M. Kogan, and M. J. Solomon, Phys. Rev. E. **77**, 050401 (2008).
[18] S. Ramakrishnan, V. Gopalakrishnan, and C. F. Zukoski, Langmuir **21**, 9917 (2005).
[19] H. Guo, S. Ramakrishnan, J. L. Harden, and R. L. Leheny, J. Chem. Phys. **135**, 154903 (2011).
[20] S. Ramakrishnan and C. F. Zukoski, Langmuir **22**, 7833 (2006).
[21] A. S. Negi, C. G. Redmon, S. Ramakrishnan, and C. O. Osuji, J. Rheol. **58**, 1557 (2014).
[22] R. N. Zia, B. J. Landrum, and W. B. Russel, J. Rheol. **58**, 1121 (2014).
[23] Z. Varga, G. Wang, and J. Swan, Soft Matter **11**, 9009 (2015).
[24] H. Tanaka and T. Araki, Phys. Rev. Lett. **85**, 1338 (2000).
[25] E. Moghimi, A. R. Jacob, N. Koumakis, and G. Petekidis, Soft Matter **13**, 2371 (2017).
[26] Q. Zhang, E. M. Dufresne, P. Grybos, P. Kmon, P. Maj, S. Narayanan, G. W. Deptuch, R. Szczygiel, and A. Sandy, J. Synchrotron Radiat. **23**, 679 (2016).
[27] P. Grybos, P. Kmon, P. Maj, and R. Szczygiel, IEEE T. Nucl. Sci. **63**, 1155 (2016).
[28] S. Romer, F. Scheffold, and P. Schurtenberger, Phys. Rev. Lett. **85**, 4980 (2000).
[29] S. Romer, C. Urban, H. Bissig, A. Stradner, F. Scheffold, and P. Schurtenberger, Phil. Trans. R. Soc., A **359**, 977 (2001).
[30] H. Bissig, S. Romer, L. Cipelletti, V. Trappe, and P. Schurtenberger, Phys. Chem. Comm. **6**, 21 (2003).
[31] R. J. M. d'Arjuzon, W. Frith, and J. R. Melrose, Phys. Rev. E **67**, 061404 (2003).
[32] A. M. Puertas, M. Fuchs, and M. E. Cates, Phys. Rev. E **75**, 031401 (2007).
[33] A. Duri and L. Cipelletti, EPL **76**, 972 (2006).
[34] G. Foffi, E. Zaccarelli, S. Buldyrev, F. Sciortino, and P. Tartaglia, J. Chem. Phys. **120**, 8824 (2004).
[35] P. Ramírez-González and M. Medina-Noyola, Phys. Rev. E **82**, 061504 (2010).
[36] See Supplemental Material at [url] for: 1. Technical details on sample preparation, XPCS and rheology measurements, and XPCS data analysis; 2. Results from sample of 56 nm radius colloids; and 3. Analysis of the temperature-dependence of gel formation time using alternative models. The Supplemental Material includes Ref. [46–55].

[37] L. B. Lurio, D. Lumma, A. R. Sandy, M. A. Borthwick, P. Falus, S. G. J. Mochrie, J. F. Pelletier, M. Sutton, L. Regan, A. Malik, and G. B. Stephenson, Phys. Rev. Lett. **84**, 785 (2000).
[38] S. Ramakrishnan, Y. L. Chen, K. S. Schweizer, and C. F. Zukoski, Phys. Rev. E. **70**, 040401 (2004).
[39] S. Romer, H. Bissig, P. Schurtenberger, and F. Scheffold, EPL **108**, 48006 (2014).
[40] Only $QR \lesssim 3$ can be measured because the scattering is too weak and the dynamics too fast for us to measure for QRs greater than this.
[41] A. Zaccone, H. H. Winter, M. Siebenbürger, and M. Ballauff, J. Rheol. **58**, 1219 (2014).
[42] A. Zaccone, J. J. Crassous, B. Béri, and M. Ballauff, Phys. Rev. Lett. **107**, 168303 (2011).
[43] A. Zaccone, J. J. Crassous, and M. Ballauff, J. Chem. Phys. **138**, 104908 (2013).
[44] J. Taffs, A. Malins, S. R. Williams, and C. P. Royall, J. Chem. Phys. **133**, 244901 (2010).
[45] C. P. Royall and A. Malins, Faraday Discuss. **158**, 301 (2012).
[46] W. Stober, A. Fink, and E. Bohn, J. Colloid Interface Sci. **26**, 62 (1968).
[47] G. H. Bogush, M. A. Tracy, and C. F. Zukoski, J. Non-Cryst. Solids **104**, 95 (1988).
[48] A. K. Vanhelden, J. W. Jansen, and A. Vrij, J. Colloid and Interface Sci. **81**, 354 (1981).
[49] A. R. Sandy, X. Jiao, S. Narayanan, and M. Sprung, AIP Conf. Proc. **879**, 898 (2007).
[50] A. R. Sandy, L. B. Lurio, S. G. J. Mochrie, A. Malik, G. B. Stephenson, J. F. Pelletier, and M. Sutton, J. Synchrotron Radiat. **6**, 1174 (1999).
[51] K. Schätzel, Quantum Opt. **2**, 287 (1990).
[52] K. Schätzel, in *Dynamic light scattering: The method and some applications*, edited by W. Brown (Clarendon Press, Oxford, 1993).
[53] L. Cipelletti and D. A. Weitz, Rev. Sci. Instrum. **70**, 3214 (1999).
[54] D. Magatti and F. Ferri, Appl. Opt. **40**, 4011 (2001).
[55] C. J. Rueb and C. F. Zukoski, J. Rheol. **41**, 197 (1997).